NASA/TM—2018-219870 AIAA–2018–1883

Examination of Wave Speed in Rotating Detonation Engines Using Simplified Computational Fluid Dynamics

Daniel E. Paxson
Glenn Research Center, Cleveland, Ohio

April 2018

NASA STI Program . . . in Profile

Since its founding, NASA has been dedicated to the advancement of aeronautics and space science. The NASA Scientific and Technical Information (STI) Program plays a key part in helping NASA maintain this important role.

The NASA STI Program operates under the auspices of the Agency Chief Information Officer. It collects, organizes, provides for archiving, and disseminates NASA's STI. The NASA STI Program provides access to the NASA Technical Report Server—Registered (NTRS Reg) and NASA Technical Report Server—Public (NTRS) thus providing one of the largest collections of aeronautical and space science STI in the world. Results are published in both non-NASA channels and by NASA in the NASA STI Report Series, which includes the following report types:

- TECHNICAL PUBLICATION. Reports of completed research or a major significant phase of research that present the results of NASA programs and include extensive data or theoretical analysis. Includes compilations of significant scientific and technical data and information deemed to be of continuing reference value. NASA counter-part of peer-reviewed formal professional papers, but has less stringent limitations on manuscript length and extent of graphic presentations.

- TECHNICAL MEMORANDUM. Scientific and technical findings that are preliminary or of specialized interest, e.g., "quick-release" reports, working papers, and bibliographies that contain minimal annotation. Does not contain extensive analysis.

- CONTRACTOR REPORT. Scientific and technical findings by NASA-sponsored contractors and grantees.

- CONFERENCE PUBLICATION. Collected papers from scientific and technical conferences, symposia, seminars, or other meetings sponsored or co-sponsored by NASA.

- SPECIAL PUBLICATION. Scientific, technical, or historical information from NASA programs, projects, and missions, often concerned with subjects having substantial public interest.

- TECHNICAL TRANSLATION. English-language translations of foreign scientific and technical material pertinent to NASA's mission.

For more information about the NASA STI program, see the following:

- Access the NASA STI program home page at http://www.sti.nasa.gov

- E-mail your question to help@sti.nasa.gov

- Fax your question to the NASA STI Information Desk at 757-864-6500

- Telephone the NASA STI Information Desk at 757-864-9658

- Write to:
  NASA STI Program
  Mail Stop 148
  NASA Langley Research Center
  Hampton, VA 23681-2199

NASA/TM—2018-219870 AIAA–2018–1883

Examination of Wave Speed in Rotating Detonation Engines Using Simplified Computational Fluid Dynamics

Daniel E. Paxson
Glenn Research Center, Cleveland, Ohio

Prepared for
2018 SciTech Forum
sponsored by the American Institute of Aeronautics and Astronautics
Kissimmee, Florida, January 8–12, 2018

National Aeronautics and
Space Administration

Glenn Research Center
Cleveland, Ohio 44135

April 2018

Acknowledgments

The author would like thank Keith Rein of Spectral Energies LLC, and the Air Force Research Laboratory for providing the temperature measurement data used in Figures 6 and 8 of this paper.

This report is a formal draft or working paper, intended to solicit comments and ideas from a technical peer group.

This report contains preliminary findings, subject to revision as analysis proceeds.

This work was sponsored by the Transformative Aeronautics Concepts Program.

Level of Review: This material has been technically reviewed by technical management.

Available from

NASA STI Program
Mail Stop 148
NASA Langley Research Center
Hampton, VA 23681-2199

National Technical Information Service
5285 Port Royal Road
Springfield, VA 22161
703-605-6000

This report is available in electronic form at http://www.sti.nasa.gov/ and http://ntrs.nasa.gov/

Examination of Wave Speed in Rotating Detonation Engines Using Simplified Computational Fluid Dynamics

Daniel E. Paxson
National Aeronautics and Space Administration
Glenn Research Center
Cleveland, Ohio 44135

Abstract

A simplified, two-dimensional, computational fluid dynamic (CFD) simulation, with a reactive Euler solver is used to examine possible causes for the low detonation wave propagation speeds that are consistently observed in air breathing rotating detonation engine (RDE) experiments. Intense, small-scale turbulence is proposed as the primary mechanism. While the solver cannot model this turbulence, it can be used to examine the most likely, and profound effect of turbulence. That is a substantial enlargement of the reaction zone, or equivalently, an effective reduction in the chemical reaction rate. It is demonstrated that in the unique flowfield of the RDE, a reduction in reaction rate leads to a reduction in the detonation speed. A subsequent test of reduced reaction rate in a purely one-dimensional pulsed detonation engine (PDE) flowfield yields no reduction in wave speed. The reasons for this are explained. The impact of reduced wave speed on RDE performance is then examined, and found to be minimal. Two other potential mechanisms are briefly examined. These are heat transfer, and reactive mixture non-uniformity. In the context of the simulation used for this study, both mechanisms are shown to have negligible effect on either wave speed or performance.

Nomenclature

a	non-dimensional speed of sound
a^*	reference speed of sound
a/f	air-to-fuel ratio
CEA	Chemical Equilibrium with Applications
CFD	computational fluid dynamic
CJ	Chapman-Jouguet
CPG	calorically perfect gas
e	non-dimensional entropy
h_f	fuel lower heating value
I_{spg}	gross specific impulse
K_0	non-dimensional rate constant
l	RDE circumference or PDE length
M	Mach number
p	non-dimensional pressure
p^*	reference pressure
p_1	non-dimensional pressure upstream of detonation
p_{amb}	ambient pressure
PDE	pulsed detonation engine
p_{man}	manifold pressure
RDE	rotating detonation engine

R_g	real gas constant
T	non-dimensional temperature
T^*	reference temperature
T_1	temperature upstream of detonation
T_{man}	manifold temperature
u	non-dimensional circumferential velocity
v	non-dimensional axial velocity
x	circumferential RDE distance or axial PDE distance
y	axial RDE distance
z	reactant mass fraction
ZND	Zeldovich-von Neumann-Doring
γ	ratio of specific heats
ρ	non-dimensional density
ρ^*	reference density

1.0 Introduction

The rotating detonation engine (RDE) is currently under investigation as an approach to achieving pressure gain combustion for propulsion and power systems, in a compact device. The RDE essentially consists of an annulus with one end open (or having a throat and/or nozzle) and the other end valved (typically using non-mechanical, fluidic means to promote through flow and prevent backflow). Fuel and oxidizer enter axially through the valved end. The detonation travels circumferentially. Combustion products exit predominantly axially through the open end. The majority of the fluid entering the device is passed over by the rotating detonation wave which, as a form of confined heat release, substantially raises the pressure and temperature. The fluid is then expanded and accelerated as it travels down the annulus. Ideally, the flow exiting the device has a higher average total pressure than the flow that enters (Ref. 1). The pressure gain of an RDE can be utilized to produce thrust directly, or it can be expanded through a turbine to produce additional useful work when compared to that from conventional combustors which incur a pressure loss when operating at the same inlet conditions and fuel flow rate.

Details of basic RDE operation may be found in numerous publications (e.g., Refs. 2 to 4), and will not be presented in this work. Suffice it to say, the fluid mechanics associated with RDE's are complex. This is particularly so when they are compared against those in pulse detonation engines (PDE's) (Ref. 5). The fill, detonation, and expansion portions of RDE cycles are highly coupled, and there is no canonical equivalent to the PDE's 'single-shot' operation which, in a sense, decouples portions of the operating cycle. The fact that the detonation is essentially propagating through a cross-flow also complicates the RDE flowfield. Furthermore, instrumentation of laboratory rigs to a level sufficient for ascertaining fluid phenomena is extraordinarily difficult due to the harsh environment and short time scales (Ref. 6). The end result of these complexities is that there are numerous unknowns concerning both the processes taking place inside an RDE, and the performance implications thereof.

This paper focuses on just one of these unknowns, namely, the observation that most measurements of detonation wave speed made in air breathing RDE's fall well below (i.e., as much as 40 percent below) those predicted by classical one-dimensional theory (a.k.a. the Chapman-Jouguet or CJ condition) (Refs. 7 and 8). Adding to this vexing oddity is the fact that most computational fluid dynamic (CFD) simulations of RDE's show much smaller, or even no deficits (Ref. 8). This is unique to the RDE flowfield. Nearly all PDE studies, both numerical and experimental, show wave speeds very close to the

so-called CJ speed (i.e., within 10 percent). In fact, the attainment of the CJ speed is often used as a benchmark for having achieved detonation in laboratory PDE experiments (e.g., Ref. 9).

In the present work, it is proposed that the intense, and likely very small scale turbulence, together with multiple sources of vorticity production associated with the RDE flowfield may be radically enlarging the reaction zone behind the leading shock of the detonation. This proposition is based on the experimentally validated three-dimensional, direct numerical simulation (DNS) and large eddy simulation (LES) work of References 10 to 13, all of which investigated detonations in tubes. Such planar detonations are typically well described by the one-dimensional Zeldovich-von Neumann-Doring (ZND) model (a shock followed by very thin constant area reaction zone) (Ref. 14). It is well-known however, that their structure is multi-dimensional. References 10 and 11 demonstrated that turbulence can substantially alter the otherwise regular, multi-dimensional, cellular structure of detonations. References 12 and 13 showed that, even without turbulence in the undetonated region, many detonable mixtures can develop highly irregular, nearly stochastic detonation cell structures, whereby local detonation failures occur, but where the reaction still completes via turbulent deflagration. Under these scenarios, both works showed that if the entire post-shock zone where reactions are occurring (i.e., where heat release takes place) is averaged in order to recover a one-dimensional model of the planar wave, the result is effectively a massive enlargement of the reaction zone compared to what a ZND model would yield. This is the phenomenological equivalent of reducing the reaction rate constant in a finite rate chemical reaction model from typical rates associated with a given homogeneous reacting fluid mixture. It is from this equivalence that the present work originates.

A simplified, CFD based simulation for RDE analysis and design has been developed, validated, and detailed in the literature (Refs. 15 to 19). A brief description will be provided in Section 2.0. By design, the simulation cannot possibly capture the physics which give rise to the reaction zone enlargement just described. However, it can shed light on the flowfield response to such an enlargement. In particular, the response of the detonation speed, the peak temperatures within the RDE annulus, and the specific impulse can and will be examined. It will be shown that reaction zone enlargement reduces detonation speed, and peak temperatures (consistent with experimental results) (Ref. 20), but has little effect on specific impulse. This analysis will be preceded by one showing that reaction zone enlargement has no effect on detonation speed in purely one-dimensional, PDE-like flowfields. This is also consistent with experiments and suggests that even in PDE's with high turbulence levels, and small turbulence scales, a wave speed deficit is unlikely. For completeness, two other potential wave speed altering phenomena will be briefly examined in the context of the simulation: heat transfer, and fuel/air mixture variations. Both will be shown to have little effect.

2.0 Simulation Description

The basis of the simulation is a high resolution, algorithm that integrates the quasi-two-dimensional, two-species, reactive Euler equations with source terms. One dimension represents the azimuthal direction of the RDE annulus; the other represents the axial direction. This assumes an inner to outer diameter ratio close to one. The code adopts the detonation frame of reference and deliberately utilizes a coarse grid (i.e., adds a degree of numerical diffusion) in order to eliminate the highest frequency unsteadiness (e.g., detonation cells, Kelvin-Helmholtz phenomena, etc.). The result is a flowfield solution that is invariant with time when converged. The working fluid is assumed to be a single, calorically perfect, premixed gas with only two species: reactant or product. For all results to be shown, the pre-mixture is hydrogen and air. The relevant parameters are: a specific heat ratio, γ=1.264; a real gas constant, R_g=73.92 ft-lb_f/lb_m/R; and a fuel heating value, h_f=51,571 Btu/lb_m.

The source terms contain sub-models that govern the reaction rate, momentum losses due to skin-friction, and the effects of heat transfer to the walls. Unless otherwise mentioned, skin friction and heat transfer will be neglected in this work. The reaction rate sub-model is one which is proportional to the product of the rate constant, K_0, the density, ρ, and the reactant mass fraction, z. Although this form lacks an Arrhenius-type exponential for temperature dependence, it does utilize a user defined threshold temperature, below which the reaction is not allowed to proceed. For all of the results to be shown, the threshold temperature is specified as 2.5 times the reference temperature. A simple reaction model of this type precludes capturing the cellular detonation structure, or the "galloping" (i.e., pulsating) planar detonation phenomenon necessary for its development (Ref. 21). Nevertheless, it captures effects within the flowfield that are germane to this study.

The governing equations are integrated numerically in time using an explicit, second-order, two-step, Runge-Kutta technique. Spatial flux derivatives are approximated as flux differences, with the fluxes at the discrete cell faces evaluated using Roe's approximate Riemann solver. Second-order spatial accuracy (away from discontinuities) is obtained using piecewise linear representation of the primitive variable states within the cells (MUSCL). Oscillatory behavior is avoided by limiting the linear slopes.

The simulation is implemented non-dimensionally. The non-dimensional pressure, p, density, ρ, temperature, T, and velocities, u and v are obtained by normalizing to a reference state p^*=14.7 psia, ρ^*=0.055 lb_m/ft^3, T^*=520 R, and the corresponding sound speed, a^*=1250 ft/s. The azimuthal and axial directions, x and y are non-dimensionalized by the circumference, l. The time, t, is non-dimensionalized using the reference wave transit time, l/a^*. The wave transit time is also used to normalize the reaction rate constant. Unless stated otherwise, all quantities displayed or discussed henceforth are non-dimensional. For reference, it is noted that this formulation results in an equation of state that is as follows.

$$p = \rho T \tag{1}$$

The speed of sound becomes simply

$$a = \sqrt{T} \tag{2}$$

3.0 Reaction Rate Effects in a One-Dimensional Tube

Before proceeding to the RDE environment, it is instructive to examine the simpler but related environment of the PDE. As mentioned in the introduction, PDE's do not generally exhibit wave speed deficits. The objective here is to examine whether the supposition of reduced reaction rate posited in this paper has an effect on their numerically simulated speed. To this end, a strictly one-dimensional version of the CFD code described above has been developed. It uses precisely the same interior numerical, and boundary algorithms, but operates on the one-dimensional version of the Euler equations. There are 2,000 numerical cells in the computing space, with an associated time step of 7.0×10^{-5}. The length scale used to non-dimensionalize is the tube length. Flow is from left to right (in the detonation frame of reference). The tube is open to ambient pressure on the right end. A stoichiometric mixture of hydrogen and air (a/f=34.3), at the reference temperature and pressure is fed into the left end at the analytical detonation Mach number, M=5.47. The initial conditions in the tube are such that the left and right halves are set the values shown in Table I. The right values represent the analytical post-reaction, or so called CJ state (Ref. 7). The simulation is then run sufficiently long such that all transient events are convected out of the computing space. The inflow Mach number is then adjusted manually, and the code is rerun, until the

TABLE I.—PDE TUBE INITIAL CONDITIONS

Variable	Left	Right
p	1	17.16
T	1	9.83
u	5.47	3.13
z	1	0

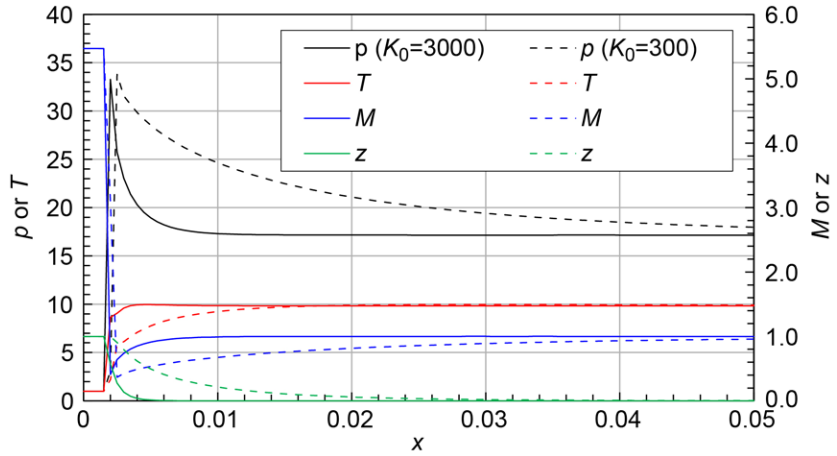

Figure 1.—Computed one-dimensional distributions of pressure, temperature, Mach number, and reactant fraction as functions of distance, in the vicinity of the reaction, for two values of the reaction rate constant.

detonation becomes stationary (i.e., the solution becomes time independent). The exit conditions are of no consequence at this point since the flow is by definition sonic at the completion of the reaction. It is noted that the boundary condition routines of the simulation are formulated to detect this situation when it occurs and to essentially neglect the imposed pressure (Ref. 15). Simulation results from following the above procedure, for two values of the rate constant, are shown in Figure 1. The two rate constants differ by an order of magnitude. For K_0=300 (dashed) and 3000 (solid), distributions of pressure, temperature, Mach number, and reactant fraction are plotted as functions of axial distance in the vicinity of the reaction.

It is seen that both simulations match all of the analytical detonation parameters correctly, including the leading shock pressure ratio of 33.3. The only difference is that the reaction zone (where $0 < z < 1$) is much larger for the lower rate constant. Note in particular that, in this one-dimensional case, the detonation speed is unchanged by the change in reaction rate. This makes physical sense if one considers the process of heat addition at constant cross-sectional area (the basis of the ZND model). Distributing the heat addition over a longer length changes nothing since the fluid is confined by the same shock on one side, and a sonic condition on the other. In fact, it can be shown (though it is not done in this work) that if the length scale in the Figure 1 profiles is changed from the tube length to the so-called reaction half-width (the distance from wherever the reaction commences to where half of the reactant mass fraction has been consumed), the K_0=300 and 3000 profiles are identical (Ref. 21). Not surprisingly then, the high fidelity numerical schemes of References 12 and 13, along with countless PDE experiments show that in tubes (i.e., planar detonations), as long as detonations are achieved, they travel at the CJ speed (Ref. 22).

It should be noted that the distributions in Figure 1 do not show the familiar induction zone which normally exists between the leading shock and the commencement of the reaction (Ref. 13). A simple

reaction scheme such as the one used here cannot capture this zone; however, its absence does not fundamentally change the results.

4.0 Reaction Rate Effects in an Idealized RDE

Consideration is now turned to the case of the idealized RDE. This is an RDE which has no viscous losses or heat transfer effects. A premixed fuel and air combination is admitted isentropically from a manifold, through the inlet end, as long as the pressure just inside the RDE is below the manifold pressure. Where the pressure just inside the RDE is above the manifold pressure (i.e., immediately behind and some distance aft of the detonation), backflow into the inlet is prevented by a notional valve that closes instantaneously (Ref. 15). The azimuthal component of the velocity at the inlet is prescribed. It represents the detonation velocity, which is unknown. As such, an iterative process must be followed as described in Reference 15 whereby the prescribed velocity is altered until the computational domain becomes time invariant. As in the previous example, a stoichiometric mixture of gaseous hydrogen and air is used. Unlike the previous example, there is no uniform state of the flow upstream of the detonation that can be stated as the initial condition. The only uniform state which can be assumed is the inlet manifold which is held at a temperature and a pressure of T_{man}= 536 R, and p_{man}= 8 Atm., respectively. The exit static pressure boundary condition is p_{amb}= 1 Atm. Symmetry boundary conditions are imposed on the left and right vertical faces of the grid in order to duplicate the continuous nature of the RDE annulus. The grid used has 400 cells in the azimuthal direction, x, and 80 cells in the axial direction, y. The non-dimensional time step is 5.0×10^{-5}.

This grid spacing is considerably coarser than that used for the one-dimensional tube simulations. Two-dimensional CFD solutions require substantially more computational resources than the one-dimensional variety, and each increment of grid refinement compounds the resource requirements exponentially (e.g., halving the grid spacing quadruples the number of numerical cells, and doubles the number of times steps required to simulate a given period). The grid spacing used represents a compromise, chosen in order to complete all the computations required for this work in a timely manner and still show appropriate trends from varying the reaction rate constant.

Figure 2 shows the stationary simulation solution for the RDE described in the form of temperature contours using a reaction rate constant of K_0=780. Also shown in the figure are distributions of axial Mach number (M_y) and normalized pressure at the inlet (bottom) and exit (top) planes. Although this notional RDE is axially shorter than most presented in the literature, it is clear from the exit plane distribution that the flow has become sonic or supersonic all along the plane and cannot expand further within the annulus. As such, and as shown in Reference 15, adding axial length at constant cross section will not improve thrust.

It is noted that the reaction rate constant chosen here is the largest value possible in the present simulation for this grid spacing. Values higher than this result in nearly all of the reaction occurring in only a few numerical cells. This in turn leads to extreme gradients and either non-physical solutions, or numerical instability.

The Figure 2 temperature contour also shows a shear region between fresh charge and burned gas where a small amount of deflagrative combustion takes place. This region is a naturally occurring part of virtually all RDE cycles. Control of its extent in the context of the present simulation is discussed in Reference 15. For all of the results to be presented it was controlled to maintain a constant detonation height (h in Figure 2).

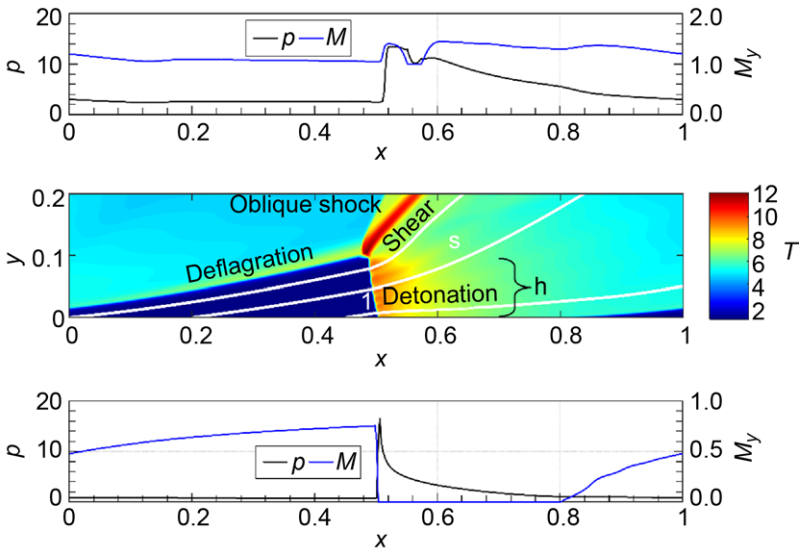

Figure 2.—Computed contours of normalized temperature throughout the annulus of the idealized RDE, in the detonation frame of reference. Axial Mach number and pressure distributions are also shown at the inlet and exit plane at the bottom and top of the figure, respectively.

Three streamlines are traced on the temperature contour of Figure 2 (white lines). These follow a particle as it enters the RDE, passes through the detonation, and exits. In order to compare results with Figure 1, the fluid states and Mach numbers along the center streamline, *s*, are shown in Figure 3. Figure 3(a) corresponds to the Figure 2 flowfield. Figure 3(b) corresponds to the Figure 2 geometry, parameters, and boundary conditions, but with K_0 reduced by a factor of 6 to 130. No temperature contour is shown for this simulation as it is virtually indistinguishable from Figure 2. The pressures and temperatures in these plots are normalized by the respective values just in front of the detonation (i.e., the white number 1, in the contour plot of Figure 2). Since the RDE flowfield is two-dimensional, both the axial and circumferential (M_x) components of Mach number are shown. Also shown are the pressure ratio, temperature ratio, and the shock Mach number corresponding to the theoretical one-dimensional CJ values. Comparing the (a) and (b) plots of this figure to that of Figure 1 yields some significant contrasts. Both Figure 3(a) and (b) yield shock Mach numbers (i.e., $\sqrt{M_x^2 + M_y^2}$) below the analytical CJ value. However, the Mach number corresponding to the high reaction rate constant simulation (Figure 3(a)) is just 4 percent below, whereas that the lower reaction rate constant is 18 percent below. The peak pressures shown in both plots of Figure 3 are lower than that of Figure 1. This is partly due to an artifact of the coarser grid used for the RDE simulations which, in combination with a reaction model without an induction zone, can miss the shock peak (Ref. 23). Although the results are not shown here, when the one dimensional model is run for the Figure 1 test problem using the RDE simulation grid spacing and reaction rate, lower peak pressures are observed; however, the detonation speed remains the same, as does the post-reaction CJ state.

Examination of the streamlines in Figure 2 suggests at least a partial explanation for the detonation wave speed variations shown in Figure 3. It is clear that the streamlines diverge after passing through the leading shock. This implies that heat addition no longer takes place at constant area as in the planar detonation case (where streamlines cannot diverge by definition). The lower the reaction rate, the more area change can occur. The area change, and in particular the enlargement allows greater expansion with

heat addition. This leads to a kind of reduced confinement which lowers the peak temperature, and post-reaction pressure, which in turn reduces the leading shock strength (i.e., detonation) speed.

A low order, essentially algebraic analysis of the so called lateral detonation area relief effect is presented in Reference 24. Using some simplifying assumptions on a quasi-one-dimensional control volume that encompasses the leading shock and the entirety of the reaction zone, the analysis yields a reduction in shock speed if the area increases in the direction of flow. However, the analysis simply assumes area change, and does not explain how it might come about. The present results provide a kind of mechanism with the notion of a lower effective heat release rate and diverging streamlines.

It is noted that the Reference 24 work requires somewhat larger changes in area than those observed here in order to achieve the same reductions in detonation speed. This may be due to simplifications and/or assumptions of the low order model. For example, the Reference 24 model assumes that, like the one dimensional detonation, the Mach number of the fluid in the detonation frame of reference is 1 just as the reaction completes. This is nearly true in Figure 3(a) where K_0=780 (see the values of M_x and M_y at s≈0.31 when z=0). However, in Figure 3(b) where K_0=130, the Mach number when z reaches 0 is seen to be approximately 1.6.

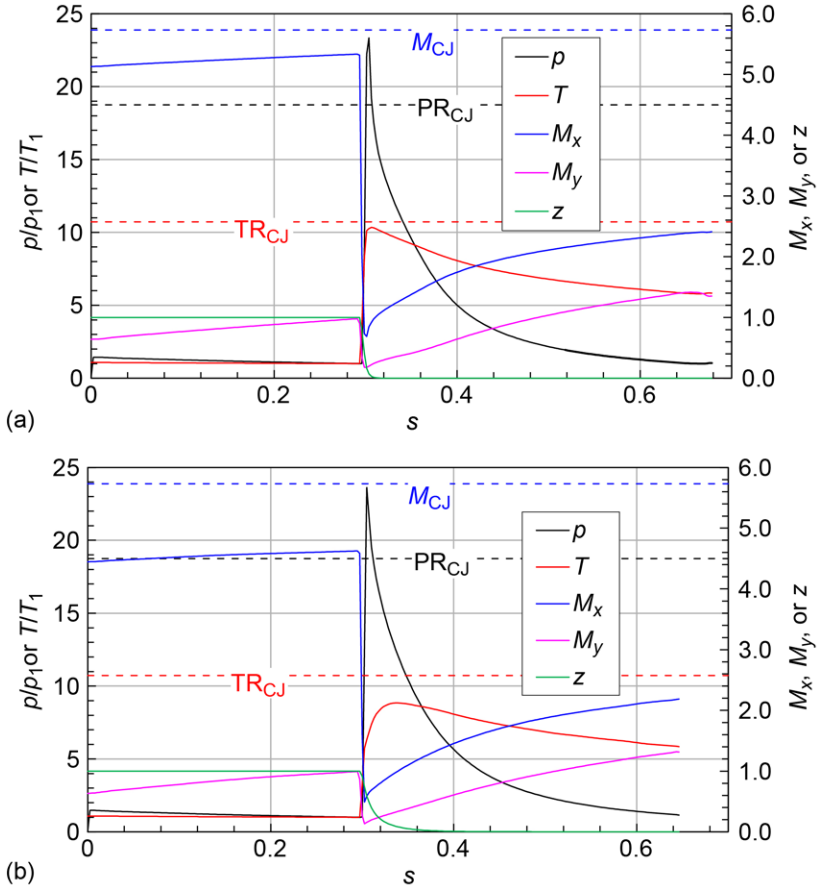

Figure 3.—Computed distributions of pressure, temperature, axial and circumferential Mach number, and reactant fraction as functions of distance along the Figure 2 center streamline, for two values of the reaction rate constant: (a) K_0=780; (b) K_0=130.

It is interesting to note the quite different working fluid states in Figure 3(a) versus Figure 3(b) at the point that the reaction completes. At first glance, it might be suspected that the availability for work or thrust production might be quite different as well. However, if the entropies along the respective center streamlines are examined, as shown in Figure 4, it is seen that the increase associated with different shock strengths, heat addition rates, and streamtube area changes, are the same. As such, it should be expected that the thrust capability of both simulations are quite similar. In this figure, the entropy is relative to the reference state and is written as follows.

$$e = \frac{\gamma}{\gamma - 1}\ln(T) - \ln(p) \tag{3}$$

That thrust capability is largely unchanged is illustrated in Figure 5. Here, the detonation circumferential Mach number (i.e., the component that could be measured in a laboratory experiment) and computed gross specific impulse are shown as functions of the reaction rate constant for the Figure 2 RDE configuration. The detonation Mach number is shown as a percentage of the one-dimensional CJ value. It is seen that the higher the reaction rate value used, the closer to the CJ value the detonation approaches. The minimum rate constant is limited in the simulation. Below a certain value (likely dependent on grid resolution and prescribed threshold temperature) the detonative structure fails. Since this paper is focused on a trend rather than a limit, and since the simplified computational model used here is not appropriate for establishing actual limits, a systematic exploration of the minimum rate constant was not pursued. Still, it is interesting to note that speeds which have been observed in experiments are shown in this figure. It is also interesting to observe that, as with the Reference 24 results, lower detonation speed has almost no impact on performance as measured by specific impulse. The exception to this latter observation is the lowest reaction rate result, which shows an approximately 5 percent reduction in specific impulse. One reason for this reduction may be that the reaction is so slow that not all of the fuel is consumed. An examination of this simulation at the exit plane revealed that approximately 7 percent of the outgoing flow was unreacted. Whether or not something like this actually occurs in some laboratory RDE's is an open question, but it is not an unreasonable supposition.

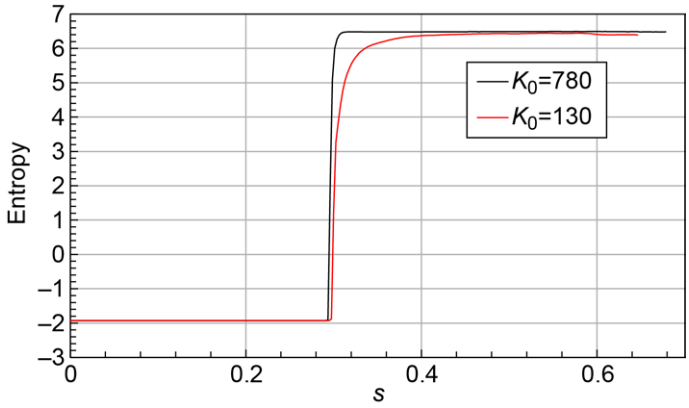

Figure 4.—Computed distributions of entropy as functions of distance along the Figure 2 center streamline, for two values of the reaction rate constant.

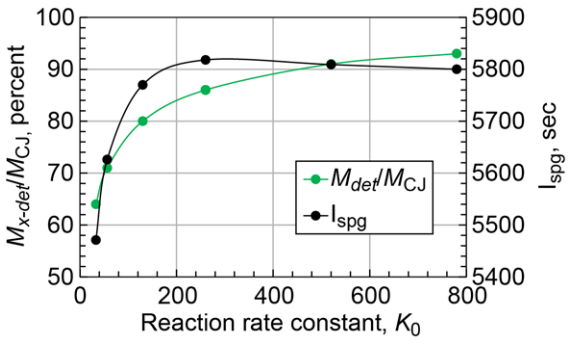

Figure 5.—Computed detonation speed and gross specific impulse as functions of reaction rate constant in the idealized RDE of Figure 2.

4.1 Corroborating Experimental Results

The observation of reduced peak temperatures (Figure 2) accompanying the reduced wave speeds calculated by the reduced reaction rate model provides an opportunity for limited corroboration with experimental results. Time resolved, line-of-sight measurements of temperature were made across the channel of an optically accessible laboratory RDE using water absorption spectroscopy in 2017 (Ref. 20). The hydrogen/air RDE was nearly identical to one used in 2015 to obtain detailed time-averaged pressure and thrust measurements (Ref. 6). The thrust and pressure results were also compared with predictions from the RDE simulation used in the present work (with all sub-models for non-ideal flow active). The comparison was quite favorable. Besides matching thrust and multiple time-averaged pressures, the mass flow rate, and the detonation wave speed matched well too. As such, an additional comparison was made in 2017 between the measured and computed temperatures.

Figure 6 shows the measured temperature at three axial locations over the course of 10 revolutions of the detonation. These 10 cycles were phase-locked based on a rising-edge temperature threshold. They were then ensemble-averaged to produce a single-cycle representative temperature profile for each location.

The computed flowfield for this RDE is shown in Figure 7 in the form of temperature contours. Some of the modelled non-ideal phenomena are labeled in the figure. Others are discussed in Reference 6. Note that Figure 7 is in the detonation frame of reference, but it is a simple matter to convert to time in the laboratory frame by dividing each circumferential location by the detonation speed used to obtain the stationary solution. The three horizontal white lines in Figure 7 represent the axial locations where the measurements were made.

Computed and ensemble-averaged measured temperatures are shown in Figure 8 at the three axial locations. Also shown is the theoretical temperature at the one dimensional CJ point as calculated by the Chemical Equilibrium with Applications (CEA) code (Ref. 25) and using the calorically perfect gas (CPG) assumption of the present simulation.

Given the uncertainties in the experimental approach (e.g., it was not validated in a detonative flowfield where the temperatures are known), and the stated simplifications of the simulation, the agreement is quite good. The computed and measured profiles have similar shapes, and the peak values compare favorably. Important to this paper is the observation that the peaks are well below the CJ value, just as the low effective reaction rate proposition predicts. It is noted that the legend of Figure 8 shows an experimental trace at 0.25 in., and a computed trace at 0.32 in. downstream from the head end. This computational location represents the closest numerical grid point to the measurement location.

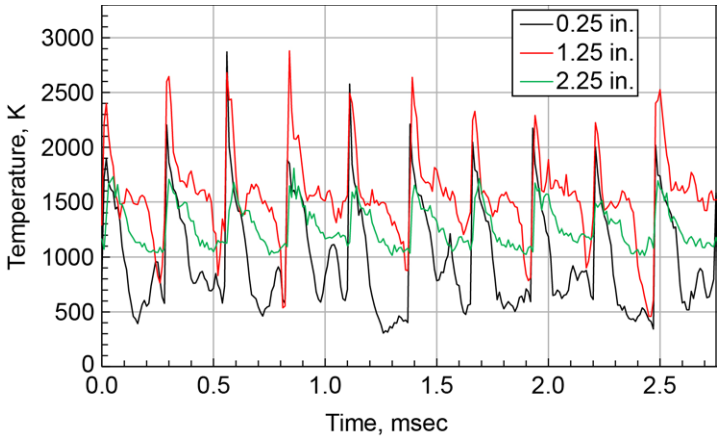

Figure 6.—Measured temperature in an RDE at three axial locations over the course of 10 rotations of the detonations.

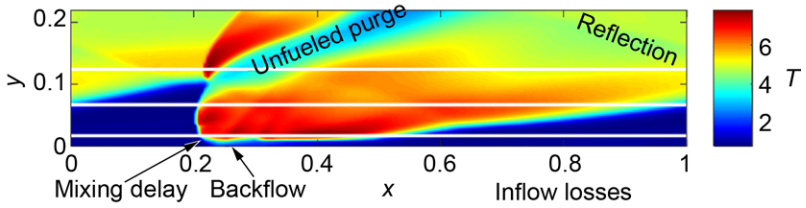

Figure 7.—Computed temperature contours for the experimental RDE of References 5 and 19. The three axial measurement locations of Reference 19 are shown as white lines.

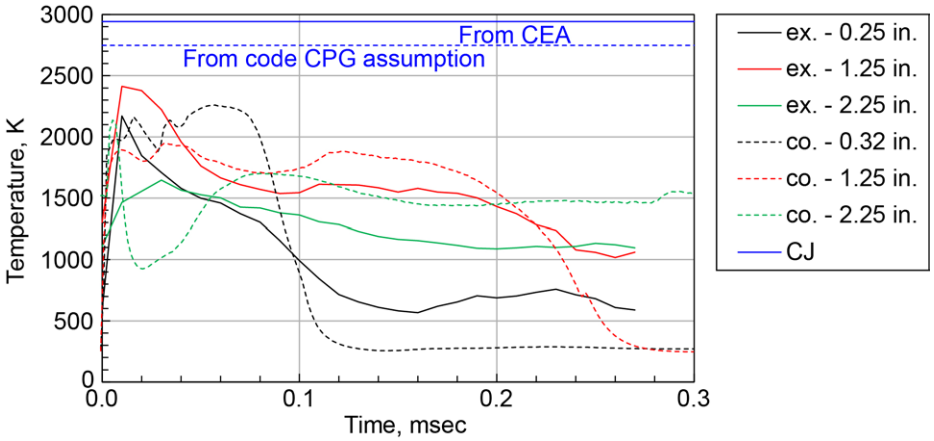

Figure 8.—Computed and Measured temperature in an RDE at three axial locations. Legend abbreviations: ex. = experimentally measured; co. = computed.

Many of the disparities between measurement and computation can be at least qualitatively attributed to modeling simplifications. For example, it is noted that the peak values and shapes of the computed and measured traces are quite different between 0 and 0.1 msec. for the 2.25 in. axial location. Figure 7 shows that this location is one of the most fluidically complex, passing through the oblique shock, and two gas interfaces. The location of this oblique shock and the extent of the purge region defining the location of the interfaces are both controlled by input parameters of the simulation. As such, changes in those parameters can greatly modify the nature of the computed trace. Furthermore, the entire contour seen in Figure 7 can essentially be shifted axially by the user specified mixing delay. This is relevant since,

although not shown, a temperature trace taken at the 1.9 in. axial position of Figure 7 showed only a single peak at 0.07 msec. with a value of 1720 K.

The shape disparity of measured and computed traces between 0 and 0.1 msec. at the 0.25 in. axial location may also be explained somewhat by the specified mixing delay. If the mixing delay were longer (or there was less backflow), the cooler, unburned flow would replace the hot flow that passes the measurement location between $0.3<x<0.5$ seen in Figure 7 (corresponding to $0.04<t<0.09$ msec. in Figure 8).

It is noted in closing this section that none of the disparities described (and potentially explained) above pertains to the trace at the axial location of 1.25 in. This location is critical as it is seen in Figure 7 to pass directly through the reaction region. The peak temperature is determined solely by the heat release. The fact that this trace is also the one with the best match between code and experiment somewhat bolsters the argument that the latter corroborates the former.

5.0 Other Contributing Factors

To be fair, there are alternative ideas to explain the low wave speeds and/or measured peak temperatures. Two of the more prominent will be considered below.

5.1 Heat Transfer

One obvious possibility is heat tranfer. RDE's typically have higher surface to volume factors than PDE's. It stands to reason that heat transferred to the wall will manifest itself as an effective loss in fuel heating value, particularly for the short duration, heat-soak, cold-wall operation that typifies most RDE experiments. A lower heating value should lower both wave speed and peak temperature.

The simulation used here has a heat transfer sub-model that has produced reasonable agreement with experimental heat flux measurements (which can span an astonishing 6 orders of magnitude over the course of a particle path through the RDE) (Ref. 17).

The Figure 2 RDE configuration with K_0=780 was run with and without this sub-model activated. Note that the heat transfer sub-model requires dimensional knowledge of the RDE (channel width, mean diameter, axial length), as well as fluid properties (viscosity, Prandtl Number, etc.). Values consistent with the experiment on which the model was validated were used. It was found that the detonation wave speed was lowered by less than 1 percent and the peak temperature along the *s* streamline of Figure 2 was lowered by 0.4 percent. This is considered negligible. In the context of the present simulation then, heat transfer is not a significant contributor to the phenomena of interest.

5.2 Non-Uniform Mixtures

Computational RDE models that show the greatest detonation wave speed deficits (i.e., closer to values measured in the laboratory) tend to attribute them to fuel and air mixing phenomena (Refs. 26 and 27). While there is undoubtedly a mixing effect, it is interesting to note that some of the largest measured deficits occur in premixed experiments (Ref. 8). These two observations may not actually be at odds. The computational models, while considerably more sophisticated (and of higher resolution) than the one used in this study, still may not be able to capture the details of the flowfield that lead to the reaction zone enlargement shown in References 10 and 13. Thus, they are unlikely to produce wave speed reductions in a premixed computation using chemistry based rate constants. However, if those same models are used to simulate the more typical non-premixed RDE's where the fuel and air are injected separately, then it is possible that variations in air/fuel ratio may lead to variations in burning rate and yield the same reaction zone enlargement effect that is posited here.

Given the inviscid, and premixed nature of the simulation used here, the only issue that can be addressed is whether variation in the reactant air/fuel ratio (i.e., variations in z) affect the computed wave speed. Furthermore, since the simulation cannot accommodate rich mixtures, only variations from lean to stoichiometric can be examined. Despite these limitations however, the exercise is a valuable one since, as will be shown, the outcome further strengthens the reduced reaction rate mechanism for low wave speed posited here.

Only the largest possible variation in air/fuel ratio will be examined. In particular, both PDE and RDE flowfields will be considered where the value of z entering the devices varies between 0 and 1. The variation will be spatial and temporal for the PDE, and only spatial for the RDE. The degree of z variation means that portions of the flowfield can potentially sustain a stoichiometric detonation front, while others cannot sustain a detonation of any kind because there is no reactant present. The goals are to examine resulting numerical solution to see if some sort of stationary, conglomerate wave structure results, and if so to see how its propagation speed compares to a detonation propagating through a flow of uniform z equal to the average of the varying z flow. Ideally, the z variation would be random, since this is likely to more closely resemble the real world. In this work however, a regular (i.e., periodic) variation is used due to ease of implementation. It is expected, though it is not proved, that results are the same.

5.2.1 PDE

Consider the same basic PDE tube arrangement used in Figure 1, except the reactant mass fraction introduced in the inlet is z=0.5. This corresponds to specifying an equivalence ratio of 0.493. According to one dimensional theory, this should lead to a stationary solution when the incoming velocity u=3.99 (note that this is also the Mach number based on the non-dimensionalization scheme and reference state used here). The CJ point, when the reaction is complete should yield p=9.33, T=5.47, M=1.0, z=0. A one-dimensional simulation similar to that used for Figure 1 confirms these values. The simulation used 400 numerical cells, and a reaction rate constant of K_0=200. Results are not shown since they differ from those of Figure 1 only in magnitude.

The two-dimensional simulation was then configured to emulate a PDE tube. Wall boundary conditions were specified for y=0.0, and y=0.2. Supersonic inflow conditions were specified at x=0.0. Constant pressure boundary conditions were applied at x=1.0. A 400 by 80 cell grid was used, just as that for Figure 2. The specified value of z at x=0.0 was varied between 0.0 and 1.0 in a sinusoidal manner from $0.0<y<0.2$. The wavelength was 0.05. The value of z was also varied temporally following a sinusoidal pattern. The mean value of z at x=0.0, from $0.0<y<0.2$ was always 0.5. The simulation was initiated in a similar manner to the one dimensional version described earlier. After initiation, it was run, and the inflow velocity was adjusted until the resulting detonation was stationary. The solution, at a moment in time, is shown in Figure 9 in the form of contours of z, Log(p), T, and M_x. The inflow velocity required to maintain a stationary (albeit wavey) detonation front was u=4.00. This is nearly identical to the theoretical value (u=3.99) for a uniform flow at z=0.5. Similarly, the post-reactive, mass-averaged pressure and temperature are 9.84 and 5.53, respectively. The variation in z can be seen in the upper left of the figure. These results indicate that for the confined PDE tube environment, and in the context of this simplified simulation, even gross non-uniformities in the mixture reactant fraction yield a stable detonation-like wave which propagates at the same speed as the uniform z detonation.

It is noted in passing that the distortion of hot and cold pockets seen in the temperature contour results from Kelvin-Helmholtz instabilities that arise from shearing. This is an inviscid phenomenon, and should occur in a properly formulated simulation. Thus, its observation gives a kind of indirect confidence in the present code. The subsequent dissipation of the distortions is numerical, and results from the coarseness of the grid.

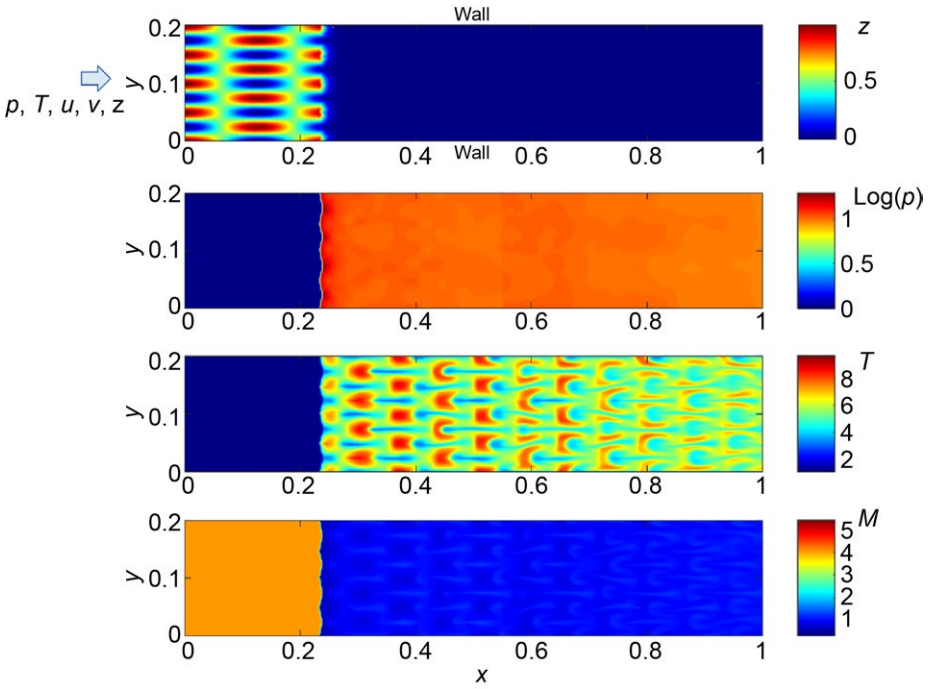

Figure 9.—Computed contours of normalized reactant fraction, Log(*p*), temperature, and Mach number throughout a two-dimensional PDE tube simulation.

5.2.2 RDE

A similar reactant fraction variation was simulated with the ideal RDE configuration of Figure 2. A stationary solution was found for a uniform reactant fraction of z=0.5 at the inlet (i.e., y=0.0). A value of K_0=260 was used. The imposed detonation speed required to obtain the stationary solution was u=3.50. This is 87 percent of the one-dimensional detonation speed, which is consistent with Figure 5. Contours of z and T are shown in Figure 10(a) for this simulation.

The same simulation was then run with a sinusoidally imposed variation $0.0<z<1.0$, where the average was z=0.5. The wavelength was 0.1. No temporal z variation was imposed. The imposed detonation speed required to obtain the stationary solution was u=3.45; nearly identical to the uniform z simulation. Contours of z and T are shown in Figure 10(b). Both simulations shown in Figure 10(a) and (b) produced identical specific impulse values of 8,112 sec. As with the PDE case, it appears from these results that detonation speed is unaffected by non-uniform reactant fraction.

It is noted that the imposed variation in z of Figure 10(b) is not convected well from the inlet at y=0.0 to the detonation front. There is significant smoothing of the gradients which is more pronounced the longer the particle path. This is partly due to the large degree of shearing that is present between the post-reactive fluid, and the entering reactant. Mostly however, it is a consequence of numerically convecting an interface diagonally on a coarse rectangular grid. Despite this smoothing however, variation in z does persist up to the detonation front. Therefore the conclusion of this section holds.

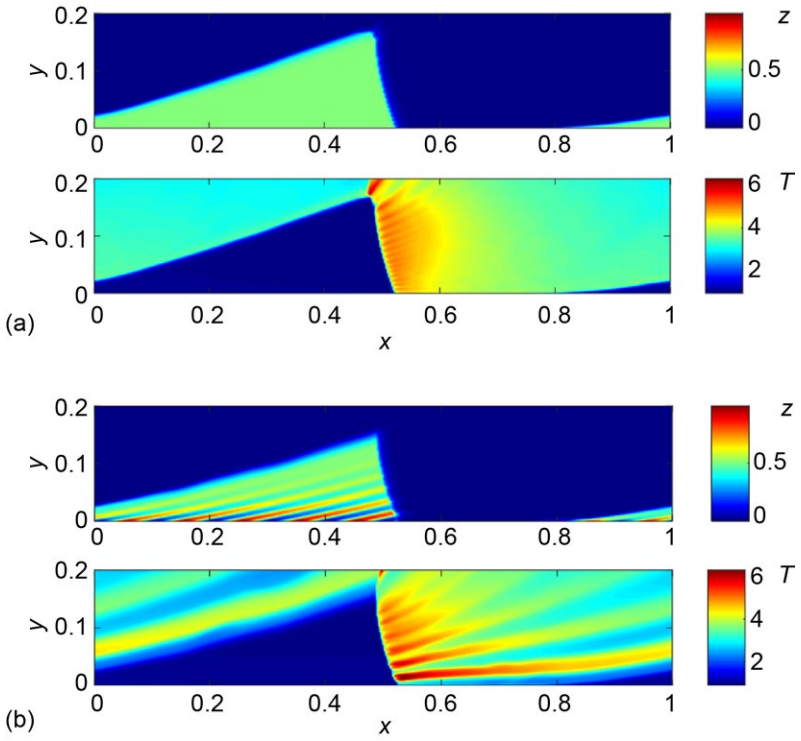

Figure 10.—Computed contours of reactant fraction and temperature in and ideal RDE with: (a) z=0.5; (b) 0.0<z<1.0 varying sinusoidally.

6.0 Conclusion

A numerical investigation has been presented which examines possible causes for the low detonation speeds observed in air breathing rotating detonation engine (RDE) experiments. These speeds are typically 15 to 40 percent below the speed predicted by one-dimensional Chapman-Jouguet theory. Using a simplified two-dimensional computational fluid dynamic simulation of an idealized RDE, it has been shown that a reduced effective reaction rate, purportedly caused by turbulence induced reaction zone enlargement, produces both the experimentally observed wave speed reduction, and reduced peak temperatures (also observed experimentally). Moreover, it has been shown that the wave speed reduction is unique to the RDE, and is not seen in the related pulse detonation engine (PDE) environment. This too is consistent with experimental observations. Finally, and critically, it has been shown that the reduction in wave speed does not alter the predicted performance of idealized RDE's as measured by gross specific impulse.

References

1. Paxson, D.E., Kaemming, T.A. "Foundational Performance Analyses of Pressure Gain Combustion Thermodynamic Benefits for Gas Turbines," AIAA-2012-0770, Jan. 2012, also NASA/TM—2012-217443.
2. Schwer, D.A., and Kailasanath, K., "Numerical Investigation of Rotating Detonation Engines," AIAA 2010-6880, Jul. 2010.
3. Nordeen, C.A., et al., "Energy Transfer in a Rotating Detonation Engine," AIAA 2011-6045, Jul. 2011.
4. Paxson, D. E., "Numerical Analysis of a Rotating Detonation Engine in the Relative Reference Frame," AIAA 2014-0284, Jan. 2014.

5. Nicholls, J. A. Wilkinson, H. R., Morrison, R. B., “Intermittent Detonation as a Thrust-Producing Mechanism,” AIAA J. of Jet Propulsion, Vol. 27, No. 5, pp. 534-541, 1957.
6. Rankin, B.A., Fotia, M.L, Paxson, D.E., Hoke, J.L., Schauer, F.R., “Experimental and Numerical Evaluation of Pressure Gain Combustion in a Rotating Detonation Engine,” AIAA-2015-0877.
7. Thompson, P.A., *Compressible Fluid Dynamics*, McGraw-Hill Advanced Engineering Series, 1988, pp. 349.
8. Andrus, I.Q., et al., “Experimentation of Premixed Rotating Detonation Engine Using Variable Slot Feed Plenum,” AIAA Journal of Propulsion and Power, DOI:10.2514/1.B36261, Apr. 2017.
9. Chapin, D.M., Tangirala, V.E., Rasheed, A., Dean, A.J., “Detonation Initiation in Moving Ethylene-Air Mixtures at Elevated Temperature and Pressure,” AIAA 2006-4793, July, 2006.
10. Massa, L., Chauhan, M., Lu, F.K., “Detonation-Turbulence Interaction,” Combustion and Flame, V. 158, 2011, pp. 1788-1806.
11. Jin, T., Luo, K., Dai, Q., Fan, J., “Simulations of Cellular Detonation Interaction With Turbulent Flow,” AIAA Journal, V. 54, 2016, pp. 419-433.
12. Maxwell, B.M., et al., “Influence of Turbulent Fluctuations on Detonation Propagation,” Journal of Fluid Mechanics, Vol. 818, May 2017, pp. 646-696.
13. Radulescu, M.I., Sharpe, G.J., Chung, K.L., Lee, J.H., “The Hydrodynamic Structure of Unstable Cellular Detonations,” Journal of Fluid Mechanics, Vol. 580, 2007, pp. 31-81, DOI:10.1017/S0022112007005046.
14. Strehlow, R.A., Combustion Fundamentals, McGraw-Hill, 1984, pp. 304-315.
15. Paxson, D.E., “Numerical Analysis of a Rotating Detonation Engine in the Relative Reference Frame,” AIAA-2014-0284, Jan. 2014, also NASA/TM—2014-216634, 2014.
16. Paxson, D.E., Fotia, M.L., Hoke, J.L., Schauer, F.R., “Comparison of Numerically Simulated and Experimentally Measured Performance of a Rotating Detonation Engine,” AIAA-2015-1101, Jan. 2015.
17. Theuerkauf, S.W., Schauer, F.R., Anthony, R., Paxson, D.E., Stevens, C.A., Hoke, J.L., “Comparison of Simulated and Measured Instantaneous Heat Flux in a Rotating Detonation Engine,” AIAA 2016-1200, Jan. 2016.
18. Paxson, D.E., “Impact of an Exhaust Throat on Semi-Idealized Rotating Detonation Engine Performance,” AIAA-2016-1647, Jan. 2016, also NASA/TM—2016-219076.
19. Paxson, D.E., Naples, A. “Numerical and Analytical Assessment of a Coupled Rotating Detonation Engine and Turbine Experiment,” AIAA-2017-1746, Jan. 2017.
20. Rein, K.D., et al, “Multi-beam Temperature Measurements in a Rotating Detonation Engine Using H2O Absorption Spectroscopy,” AIAA-2017-1064, Jan. 2017.
21. Hwang, P. et al, “Numerical Resolution of Pulsating Detonation Waves,” Combustion Theory and Modelling, Vol. 4, No. 3, 2000, pp. 217-240.
22. Hopper, D.R., H.D., King, P.I., Schauer, F.R., “Propagation of Detonations Across a Step Area Change in a Pulsed Detonation Engine,” AIAA 2007-0446, January, 2007.
23. Nalim, R.M., Paxson, D.E., “A Numerical Investigation of Premixed Combustion in Wave Rotors,” ASME Journal of Engineering for Gas Turbines and Power, Vol. 119, No. 3, 1997, pp. 668-675, also ASME Paper 96-GT-116, June, 1996, also, NASA TM 107242.
24. Kaemming, T.A., Fotia, M.L., Hoke, J.L., Schauer, F.R., “Thermodynamic Modeling of a Rotating Detonation Engine Through a Reduced-Order Approach,” AIAA Journal of Propulsion and Power, DOI:10.2514/1.B36237, 2017.
25. McBride, B.J., Sanford, G. “Computer Program for Calculation of Complex Chemical Equilibrium Compositions and Applications II,” NASA-RP-1311, 1996.

26. Schwer, D.A., Kailasanath, K., “Physics of Heat-Release in Rotating Detonation Engines,” AIAA 2015-1602, Jan. 2015.
27. Cocks, P.A., Holley, A.T., Rankin, B.A., “High Fidelity Simulations of a Non-Premixed Rotating Detonation Engine,” AIAA 2016-0125, Jan. 2016.